J. Am. Soc. Mass Spectrom. (2018) 29:1781–1790
DOI: 10.1007/s13361-018-1929-7

FOCUS: APPLICATION OF PHOTONS AND RADICALS FOR MS: RESEARCH ARTICLE

Spectroscopic Identification of the Carbyne Hydride Structure of the Dehydrogenation Product of Methane Activation by Osmium Cations

P. B. Armentrout,[1] Stach E. J. Kuijpers,[2] Olga V. Lushchikova,[2] Randy L. Hightower,[1] Georgia C. Boles,[1] Joost M. Bakker[2]

[1]Department of Chemistry, University of Utah, 315 South 1400 East, Room 2020, Salt Lake City, UT 84112, USA
[2]Radboud University, Institute for Molecules and Materials, FELIX Laboratory, Toernooiveld 7c, 6525 ED, Nijmegen, The Netherlands

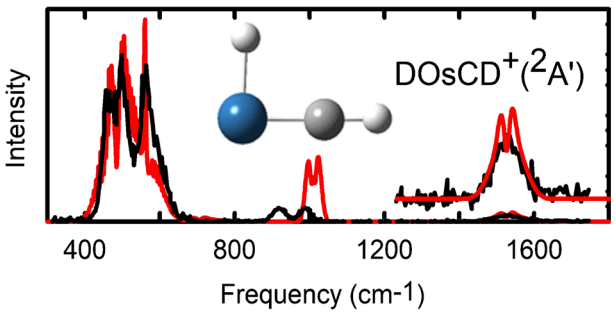

Abstract. The present work explores the structures of species formed by dehydrogenation of methane (CH_4) and perdeuterated methane (CD_4) by the 5d transition metal cation osmium (Os^+). Using infrared multiple photon dissociation (IRMPD) action spectroscopy and density functional theory (DFT), the structures of the $[Os,C,2H]^+$ and $[Os,C,2D]^+$ products are explored. This study complements previous work on the related species formed by dehydrogenation of methane by four other 5d transition metal cations (M^+ = Ta^+, W^+, Ir^+, and Pt^+). Osmium cations are formed in a laser ablation source, react with methane pulsed into a reaction channel downstream, and the resulting products spectroscopically characterized through photofragmentation using the Free-Electron Laser for IntraCavity Experiments (FELICE) in the 300–1800 cm^{-1} range. Photofragmentation was monitored by the loss of H_2/D_2. Comparison of the experimental spectra and DFT calculated spectra leads to identification of the ground state carbyne hydride, $HOsCH^+$ ($^2A'$) as the species formed, as previously postulated theoretically. Further, a full description of the systematic spectroscopic shifts observed for deuterium labeling of these complexes, some of the smallest systems to be studied using IRMPD action spectroscopy, is achieved. A full rotational contour analysis explains the observed linewidths as well as the observation of doublet structures in several bands, consistent with previous observations for $HIrCH^+$ ($^2A'$).

Keywords: Spectroscopy, Intracavity free electron laser, Infrared multiple photon dissociation, Rotational band structure

Received: 22 January 2018/Revised: 15 February 2018/Accepted: 23 February 2018/Published Online: 9 April 2018

Introduction

The functionalization of methane, the least reactive hydrocarbon and a major component of natural gas, presents a major technical challenge and opportunity. Catalysts for direct conversion of methane into liquid fuels and other valuable commodities, e.g., methanol, ethene, or ethane, would be of great technological interest [1, 2]. The development of more efficient and economical catalysts for this purpose could be aided by a better understanding of the factors that permit the activation of the inert CH bonds of methane. Gas-phase studies are potentially a valuable starting point for elucidating the intrinsic reactive properties of metals in the absence of solvent, stabilizing ligands, and metal supports. Gas-phase work also forms an ideal interface with theory, thereby yielding benchmark information that can help guide theory

Electronic supplementary material The online version of this article (https://doi.org/10.1007/s13361-018-1929-7) contains supplementary material, which is available to authorized users.

Correspondence to: P. Armentrout; *e-mail:* armentrout@chem.utah.edu

of more complex systems. Such gas-phase work has been reviewed by Schwarz [3] and by Roithová and Schröder [4].

Among the transition metal cations, none of the first-row and only Zr^+ in the second row are observed to react with methane at room temperature [3–24]. In the case of Zr^+, the reaction is inefficient because it is slightly endothermic [21]. In contrast, several 5d transition metal cations (Ta^+, W^+, Os^+, Ir^+, and Pt^+) activate methane exothermically at room temperature through dehydrogenation, yielding $[M,C,2H]^+ + H_2$ products [25–34]. This was first reported by Irikura and Beauchamp, who used a Fourier transform ion cyclotron resonance (FTICR) spectrometer [27]. Flow tube studies by Bohme and coworkers also observed this reactivity in their survey of all of the transition metal cations [24]. Guided ion beam studies, which examine this reactivity at thermal and elevated energies, have provided extensive information about the reactivity, energetics, and periodic trends of these reactions [11, 29–38].

Although such studies provide extensive information about periodic trends in the reactivity of these metal cations with methane, they do not provide any structural information. For many years, it was presumed that these species had carbene structures in which CH_2 is doubly bound to the metal and the MCH_2^+ species has C_{2v} symmetry. This conclusion was largely based on the pioneering theoretical examination of the 5d $[M,C,2H]^+$ species by Irikura and Goddard [39]. They also considered the carbyne hydride structure, $HMCH^+$, explicitly calculating the relative energies for $[Ta,C,2H]^+$ carbene and carbyne structures and finding the latter to lie significantly higher in energy. These authors discarded carbyne hydride structures for the other 5d transition metals on the basis of arguments that they cannot form the four covalent bonds needed for stability (La^+, Hf^+, Pt^+, Au^+) or that they have large losses of exchange energy (W^+, Re^+, Os^+, Ir^+). Later, structures of the $[W,C,2H]^+$ complex were examined by Simon et al. [40], who found that the carbyne hydride and carbene structures are close in energy. Further, the carbene is distorted from C_{2v} symmetry to a C_s symmetry because of agostic interactions, in which electrons in one of the C-H bonds donate into an empty metal d-orbital thereby forming a two-electron bond on the M, C, and H centers [41–43].

Recently, these theoretical predictions were experimentally tested by infrared multiple photon dissociation (IRMPD) action spectroscopy on the structures of the $[M,C,2H]^+$ products where $M^+ = Ta^+$, W^+, Ir^+, and Pt^+ [44] (and their perdeuterated analogues) [45]. Importantly, these studies utilized the Free Electron Laser for IntraCavity Experiments (FELICE) beamline, with subsequent work showing that IRMPD spectra of $[Pt,C,2H]^+$ and $[Pt,C,2D]^+$ *cannot* be achieved using the extracavity output of the normal FELIX beam lines [46]. The $[M,C,2H]^+$ systems are among the smallest molecules for which IRMPD action spectroscopy has been achieved [47–49] and the only ones studied over such a large IR spectral range. In most IRMPD studies, the general view is that molecules absorb a photon in an optically accessible vibrational coordinate and then the energy is rapidly redistributed into the molecular bath of all vibrations through intramolecular vibrational redistribution (IVR) [50, 51]. However, in a four-atom system, the IVR rate is presumably too low to allow the efficient delocalization of the vibrational energy, thereby limiting the efficient absorption of multiple IR photons. The intensity of the intracavity arrangement of the FELICE beamline overcomes this limitation.

In our previous IRMPD studies [44, 45], the ground state species for $[Ta,C,2H]^+$ and $[W,C,2H]^+$ were shown to have carbene structures distorted by agostic interactions, whereas $[Pt,C,2H]^+$ was assigned as the classic carbene structure having C_{2v} symmetry. Surprisingly, $[Ir,C,2H]^+$ exhibited a mixture of both $HIrCH^+$ and $IrCH_2^+$ structures, with the former dominating. It was shown theoretically that the carbyne hydride of iridium is indeed lower in energy than the carbene, a consequence of changing spin, which thereby empties one of the d orbitals allowing interaction with a CH bond. Spectral assignments in the $[Pt,C,2H]^+$ and $[Ir,C,2H]^+$ systems were complicated by additional bands [44], which the subsequent work on perdeuterated isotopologues indicated could be assigned to overtones [45]. The latter work also demonstrated that several features of the spectra of all four metal systems result from the rotational substructures of the vibrational bands. Although the effects of rotational structure have been observed for the photodissociation of weakly bound species [52], this study yielded the first evidence for rotational structure observed in IRMPD spectra of covalently bound species.

In the present study, the remaining 5d transition metal cation that is known to exothermically dehydrogenate methane, osmium, is examined. Early theoretical work assigned the structure of the $[Os,C,2H]^+$ product to the carbene [27, 28, 39, 53, 54]. Subsequently, we have examined the thermochemistry of this reaction using guided ion beam tandem mass spectrometry, a study that included a theoretical evaluation of the potential energy surfaces [33]. As this study followed the IRMPD work, the possibility of forming $HOsCH^+$ was explored. Indeed, the ground state structure of the dehydrogenation product was identified as $HOsCH^+$, with $OsCH_2^+$ lying higher in energy. The present spectroscopy study strongly supports the carbyne hydride as the experimentally formed species and also provides another example of the importance of evaluating the rotational band structure in IRMPD studies.

Experimental and Computational Methods

Experimental Details

IRMPD action spectroscopy experiments utilized a molecular beam apparatus connected to the first beamline of FELICE, systems described in detail elsewhere [49]. Osmium cations were created using a Smalley-type laser ablation source [55, 56]. A solid rod of a Ru/Os alloy (50/50, ACI Alloys) was rotated and translated while being irradiated with the second harmonic of a pulsed Nd:YAG laser (532 nm). This yielded a plasma constrained in a 3-mm-diameter × 60-mm-long channel by helium injected into the channel via a pulsed valve (General Valve Series 9). A second pulsed valve was used to inject

methane (CH_4) or deuterated methane (CD_4) (5% in He) into the channel approximately 50 mm downstream from the laser focal point. Approximately 20–30% of the osmium cations were found to react with methane under these conditions. Upon exiting the channel, the gas pulse expanded into vacuum and was shaped by a skimmer (2 mm diameter) and a horizontal slit aperture (8 × 2 mm), both being electrically grounded. The molecular beam then entered the intracavity region at an angle of 35° with respect to the FELICE IR laser beam. IR radiation in the 300–1800 cm^{-1} spectral range was utilized in the present experiments. FELICE produces a macropulse (typical duration of 7 μs) consisting of ps-long micropulses separated by 1 ns. The radiation used was near transform-limited, with a spectral width set to ~ 0.5% full width at half maximum (fwhm) of the central frequency (thus, 5 cm^{-1} at 1000 cm^{-1}).

In the course of traversing the apparatus, the molecular beam interacted with the IR light for several microseconds before all ions were pulse extracted into a reflectron time-of-flight (RETOF) mass spectrometer (Jordan TOF Products, Inc.; mass resolution, $M/\Delta M \approx 1700$). A 400-Msample/s 100 MHz digitizer (Acqiris DP310) was used to record transients from the multichannel plate (MCP) detector. The molecular beam was pulsed at twice the rate of FELICE, thereby permitting the acquisition of reference mass spectra, which allows corrections for long-term source fluctuations and the determination of fragments generated by irradiation with FELICE.

The experimental IRMPD spectra for $[Os,C,2H/D]^+$ were constructed by calculating the fragmentation yield, which is given by $y = -\ln[P/(P + F)]$ where F and P are the fragment and precursor ion intensities, respectively, and the fragment intensity is corrected for the presence of signal without laser irradiation (needed only for the perprotio system). Possible fragmentation to the bare Os^+ product (i.e., loss of CH_2/CD_2) was not included in these calculations because, as noted above, a substantial amount of the bare metallic cation (20–30%) did not react with the CH_4/CD_4 and was present in the molecular beam. The fragment ion yield was corrected for the IR macropulse energy, determined by coupling a fraction of the light out of the cavity. During the experiments, the typical macropulse energies amounted to 0.6–0.8 J.

Osmium has a complex set of stable isotopes (^{184}Os, 0.02%; ^{186}Os, 1.59%; ^{187}Os, 1.96%; ^{188}Os, 13.24%; ^{189}Os, 16.15%; ^{190}Os, 26.26%; ^{192}Os, 40.78%). Because of the isotopic patterns of the metals, observation of fragment ions can be obscured. Additionally, under the experimental conditions, both $[Os,C,2H/D]^+$ and small amounts of $[Os,2C,6H/D]^+$ species are formed. The latter species are stabilized through collisions with the helium carrier gas in the molecular beam. Because of the presence of the $[Os,2C,6H/D]^+$ species, it is possible that methane loss and dehydrogenation from $[Os,2C,6H/D]^+$ could interfere with the $[Os,C,2H/D]^+$ decomposition products, thereby affecting the relative intensities of the target fragments. To avoid such interferences, signals were collected using methane reactant pressures that minimized the formation of the $[Os,2C,6H/D]^+$ product. Spectra shown were obtained by monitoring fragmentation into $^{186}OsC^+ + {}^{187}OsC^+ + {}^{188}OsC^+ + {}^{189}OsC^+$ and correcting for the small amounts of $^{186}OsCH_2^+ + {}^{187}OsCH_2^+$ present without laser irradiation (no such corrections were necessary for the CD_4 system). Additionally, it was verified that depletions of the $[Os,C,2H/D]^+$ species were matched by the increase in intensities of these fragment ions. An example mass spectrum is shown for both $[Os,C,2H]^+$ and $[Os,C,2D]^+$ in Supplementary Figure S1. Previously measured thermochemistry indicates that the decomposition pathways observed are the lowest energy fragmentation routes available, here, loss of H_2/D_2, which requires $> 1.86 \pm 0.21$ eV [33]. (Loss of H requires $> 2.30 \pm 0.15$ eV, and loss of CH_2 requires > 4.71 eV. It can also be realized that these relative energetics hold for any isomer of $[Os,C,2H/D]^+$, such that loss of H_2/D_2 will be the lowest energy pathway no matter what isomer is present.) As for other late transition metals [29, 31], the decomposition pathway observed corresponds to loss of H_2/D_2 because the metal carbide bond energies of the late metals are fairly strong, a consequence of occupied 5d orbitals allowing π backbonding [34]. From these energetics, we can evaluate the minimum number of IR photons needed to induce this dehydrogenation as > 27 and > 8 photons of 500 and 1600 cm^{-1}, respectively. More photons than this minimum number are usually needed for the rate of fragmentation to be sufficiently high for observation within the 10–100 μs experimental time window.

For both $[Os,C,2H]^+$ and $[Os,C,2D]^+$, spectra were obtained both in-focus (maximum fluence) and out-of-focus to evaluate the effect of the macropulse fluence on the observed spectra. To achieve this, the entire experimental apparatus was translated along the FELICE laser beam, which allowed a reduction of up to a factor of 40 at a maximum translation of 300 mm out of focus of the FELICE optical beam with its 55 mm Rayleigh range. The variation of the fluence leads to a relatively linear dependence of the fragmentation yield once a certain threshold has been overcome, as determined previously [57, 58]. Eventually, all ions in the interaction volume (determined by the overlap between laser and molecular beams) have fragmented and saturation leads to a broadening of spectral lines. In presenting spectra both in-focus and out-of-focus, we enable the observation of the weakest resonances while also being able to observe bands without broadening effects. The range of fluences in the focus extended from 25 J cm^{-2} at 300 cm^{-1} to 150 J cm^{-2} near 1400 cm^{-1}, with estimated peak power densities ranging from 4×10^8 to 9×10^9 W cm^{-2}.

Computational Details

For comparison with the observed IRMPD experimental spectra, density functional theory (DFT) calculations were performed using the Gaussian 16 suite of programs [59] yielding predicted IR spectra for possible structures of $[Os,C,2H/D]^+$. We employed the B3LYP hybrid density functional [60, 61] and def2-TZVPPD basis set, which is a balanced triple-zeta basis set with two polarization functions and one diffuse function on all elements with an all-electron basis set for C and H and an effective core potential (ECP) for osmium [62]. The

small-core ECP basis set employed here explicitly includes the 5s, 5p, 6s, 6p, and 5d electrons. This approach is similar to that taken in the previous spectroscopic studies of $[M,C,2H/D]^+$ for $M^+ = Ta^+$, W^+, Ir^+, and Pt^+ [44, 45] and utilizes a slightly larger basis set than previous explorations of all species formed in the reaction of Os^+ with CH_4 (B3LYP/def2-TZVPP) [33]. (Notably, the change in basis set leads to very small changes (< 0.01 eV) in the relative energies of different states of $[Os,C,2H]^+$ with one exception, the $^4B_2$ state of $OsCH_2^+$. This can be traced to a large change in the vibrational frequency for the out-of-plane bend, calculated here as 1774 cm^{-1} and as 1318 cm^{-1} previously. This large change can be attributed to a change in the default grid for integral calculations from FineGrid in Gaussian 09 to Grid = Ultrafine for Gaussian 16.) For calculation of vibrational frequencies, the ^{190}Os isotope was used and zero point energies were scaled by 0.9885 [63] in the determination of relative energies. In our previous work, anharmonic frequency calculations for the Ta, W, Pt, and Ir systems yielded only small shifts in the locations of the calculated resonances. Likewise, anharmonic calculations of the two electronic states of $HOsCH^+$ and $DOsCD^+$ using second-order vibrational perturbation theory [64] show average shifts of 1.4% in the four lowest frequency modes (see Supplementary Table S1). More importantly, relative band positions vary by less than 6 cm^{-1} such that either the harmonic or anharmonic frequencies when appropriately scaled will provide the same comparisons to the data. For consistency with our previous work, the harmonic frequencies are utilized below.

The theoretical and experimental spectra were compared after scaling the harmonic frequencies of the former by a global scaling factor of 0.95 to account for anharmonicity. This factor provides reasonable agreement with the present experiments and also matches the scaling factor used previously for $[Ta,C,2D]^+$ [45]. When rotational substructure is not included, the theoretical spectra were convoluted using a Gaussian line shape function with a fwhm of 30 cm^{-1} (as utilized previously for the late transition metals, Pt and Ir) [44, 45].

Rotational Contours

In our previous work on the $[M,C,2D]^+$ systems where $M^+ = Ta^+$, W^+, Ir^+, and Pt^+ [45], we found that the spectral bands observed in IRMPD spectroscopic characterization of these systems are subject to rotational broadening. This is because the rotational constants for these small ions are of the same order as the spectral bandwidth of the exciting laser, and the experiments are performed near room temperature. (Although the expansion into vacuum could yield some cooling, the efficiency of this process is unclear and energy released in the exothermic reaction forming the irradiated species may not be dissipated completely.) Thus, a non-negligible population of excited rotational sublevels was observed to contribute to broadening of the bands in these systems. Analogous to that work, here we simulate rotational contours for each predicted vibrational band. Rotational envelopes were simulated using dedicated software to diagonalize the pure rotational Hamiltonians for a-, b-, and c-type vibrational transitions [65]. The rotational transitions were simulated by convoluting the transition dipole moments originating from a wide range of J,K states with a single temperature Boltzmann state distribution (293 K), with no change in the rotational constants between the vibrational ground and excited states. The rotational temperature was chosen to be near room temperature, which provides a reasonable match between experimental and simulated spectra (as seen below). All ro-vibrational transitions were assumed to be pure a-, b-, or c-type, which is not exact for the less symmetric species, but most bands are within 90% character of one of the three transition types. (Two of the weaker bands of $HOsCH^+$ ($^2A'$) deviate more, but these are not important in the current analysis.) Details of the information needed for these analyses are included in the Supplementary Table S2 and Supplementary Figures S2 and S3. The resulting distribution of rotational transitions was then shifted in frequency by the (scaled) harmonic frequency of the associated vibrational band and convoluted with a Gaussian lineshape function with a width of 0.3% of the central frequency, representing the spectral bandwidth of FELICE, and an amplitude given by the DFT calculated IR intensity.

It is also useful to consider the qualitative character of the various transitions. The results obtained here and previously show that a-type transitions are closest to the textbook-type spectrum of a diatomic molecule. They consist of separated P and R branches and can have contributions from a weak Q branch (strictly forbidden for a diatomic, not so strictly for polyatomics). In contrast, b- and c-types are much more complicated because of a variety of distinct ΔK_a transitions, each of which has P, Q, and R branches. This leads to rotational substructure that is a complicated superposition of P, Q, and R-branches for different K values. As such, although the b- and c-type bands appear to show structure that for a diatomic would correspond to P, Q, and R-branches, such nomenclature is incorrect here.

Results and Discussion

Theoretical Results

Table 1 lists the theoretical energies and zero point energies for several states of the $[Os,C,2H]^+$ and $[Os,C,2D]^+$ systems as calculated at the B3LYP/def2-TZVPPD level of theory. These results are similar to those previously published, where a more complete listing of other excited states is also provided [33]. Several structures are possible and include the methylidene (carbene), $OsCH_2^+$; methylidyne (carbyne) hydride, $HOsCH^+$; a carbide dihydride, $HOsHC^+$; and an adduct of the carbide with dihydrogen, $(H_2)OsC^+$. Energies relative to the $Os^+ + CH_4/CD_4$ reactants are also provided and show that only the lowest energy states of the $HOsCH^+$ species can be formed exothermically from these reagents. Formation of several $OsCH_2^+$ states is barely exothermic and barely endothermic for the $OsCD_2^+$ analogues. Note that these two species have different spin states, quartet and doublet, respectively, and that

Table 1. Calculated Electronic Energy, Vibrational Zero-Point Energy (ZPE), and Energy (E_{rel}) of $[Os,C,2H]^+ + H_2$ ($[Os,C,2D]^+ + D_2$) Products Relative to $Os^+ + CH_4$ (CD_4) Reactants

Species	State	Energy (E_h)	ZPE (E_h)[a]	E_{rel} (eV)
$Os^+ + CH_4$ (CD_4)	$^6D + {}^1A_1$	−130.822655	0.044080 (0.032319)	0.000
H_2 (D_2)	$^1\Sigma_g^+$	−1.1800213	0.009953 (0.007040)	
$HOsCH^+$ ($DOsCD^+$)	$^2A'$	−129.650291	0.020188 (0.015457)	−0.588 (−0.476)
	$^2A''$	−129.637074	0.019907 (0.015256)	−0.236 (−0.121)
$OsCH_2^+$ ($OsCD_2^+$)	$^4B_1$	−129.633815	0.023148 (0.017561)	−0.059 (0.030)
	$^4B_2$	−129.633785	0.024141 (0.018347)	−0.031 (0.049)
	$^4A_2$	−129.632238	0.022643 (0.017151)	−0.030 (0.062)
	$^4B_1$	−129.622505	0.022196 (0.016822)	0.223 (0.318)
$HOsHC^+$ ($DOsDC^+$)	$^2A'$	−129.603017	0.016868 (0.012728)	0.608 (0.736)
$(H_2)OsC^+$ ($(D_2)OsC^+$)	$^4A''$	−129.554538	0.014131 (0.010698)	1.853 (2.000)

Values for perdeuterated species in parentheses. All values obtained at the B3LYP/def2-TZVPPD level
[a]Frequencies were scaled by 0.9885 [63]

the carbenes have C_{2v} symmetry. Table 2 lists the calculated vibrational frequencies for the lowest energy $[Os,C,2H/D]^+$ species in Table 1. Although most of the frequencies and nature of vibrational modes are similar for the $HMCH^+$ carbyne hydride and MCH_2^+ carbene structures, several modes do change. The in-phase in-plane bend of $HOsCH^+$ becomes the CH_2 scissor vibration in the carbenes. The MH and CH stretches of $HOsCH^+$ become the symmetric and asymmetric stretches in the carbenes.

[Os,C,2H]$^+$

The IRMPD spectrum of $[Os,C,2H]^+$ is shown in Figure 1 and exhibits five resonances at 649, 684, 721, 1049, and 1286 cm^{-1}. A potential shoulder at ~770 cm^{-1} could also be identified as a resonance. The out-of-focus spectrum reproduces the three intense bands at the lower frequencies. To analyze this spectrum, we first compare it with those predicted for the five species that can be formed exothermically from Os^+ reacting with CH_4 (Table 1). It can be seen that either of the $HOsCH^+$ species (both the $^2A'$ ground state and low-lying $^2A''$ state) have strong resonances between 600 and 800 cm^{-1}. These correspond to the out-of-phase in-plane bend at 638 and 614 cm^{-1}, respectively, and the out-of-plane (oop) bend at 728 and 741 cm^{-1}, respectively. Note that the 90 cm^{-1} separation between these bands for the $^2A'$ state reproduces the width of the experimental band better than the 127 cm^{-1} separation of the $^2A''$ state. Further, the weak band at 1049 is reproduced by the Os-C stretch at 1064 and 1059 cm^{-1}, respectively. For these two species, the in-phase in-plane bend at 907 and 884 cm^{-1} is relatively weak, and the OsH (2154 and 2087 cm^{-1}, respectively) and CH (3025 and 3012 cm^{-1}, respectively) stretches are above the range experimentally accessible. Neither of these $HOsCH^+$ species reproduce the band observed at 1286 cm^{-1} as a fundamental, although this frequency could conceivably be associated with the overtone of the in-plane bend, as discussed further below.

In contrast, the three carbenes predict the strongest resonances for either the out-of-phase in-plane bend at 1010 cm^{-1} for the $^4B_1$ state or the out-of-plane bend at 1774 cm^{-1} ($^4B_2$) or 1021 cm^{-1} ($^4A_2$). The vibrations for these different carbene states differ appreciably because of the occupation of the

Table 2. Calculated Vibrational Frequencies (cm^{-1}) and Intensities (km mol^{-1})

Mode	Exp.	$HOsCH^+$ ($^2A'$)	$HOsCH^+$ ($^2A''$)	$OsCH_2^+$ ($^4B_1$)	$OsCH_2^+$ ($^4B_2$)	$OsCH_2^+$ ($^4A_2$)
$[Os,C,2H]^+$						
HOsCH out-of-phase in-plane bend	649, 684	638 (80)	614 (78)	*1010 (437)*	*565 (16)*	*610 (0.1)*
OsCH oop bend	721	728 (74)	741 (74)	*870 (77)*	*1774 (1609)*	*1021 (87)*
HOsCH (CH_2 scissors) in-phase in-plane bend		907 (1)	884 (6)	*1254 (0.1)*	*1261 (0.1)*	*1362 (5)*
Os-C stretch	1049	1064 (10)	1059 (10)	*718 (1)*	*724 (0.7)*	*718 (9)*
Overtone	1286	2 × 638				
OsH (CH_2) sym. stretch		2154 (5)	2087 (5)	*2875 (58)*	*2875 (59)*	*2878 (7)*
CH (CH_2) asym. stretch		3025 (133)	3012 (120)	*3037 (360)*	*2984 (42)*	*2963 (0.2)*
$[Os,C,2D]^+$						
DOsCD out-of-phase in-plane bend	461, 498	457 (39)	437 (38)	*755 (230)*		
OsCD oop bend	563	561 (39)	571 (39)	*681 (41)*		
DOsCD (CD_2 scissors) in-phase in-plane bend		707 (1.0)	693 (4)	*982 (0.2)*		
Os-C stretch	920, 990	1011 (12)	1007 (11)	*638 (0.8)*		
Overtone		2 × 457				
OsD (CD_2) sym. stretch	1528	1528 (2)	1481 (2)	*2078 (28)*		
CD (CD_2) asym. stretch		2256 (58)	2246 (52)	*2274 (249)*		

All theoretical vibrational frequencies have been scaled by 0.950. Intensities in parentheses. Values for carbene structures are in italics

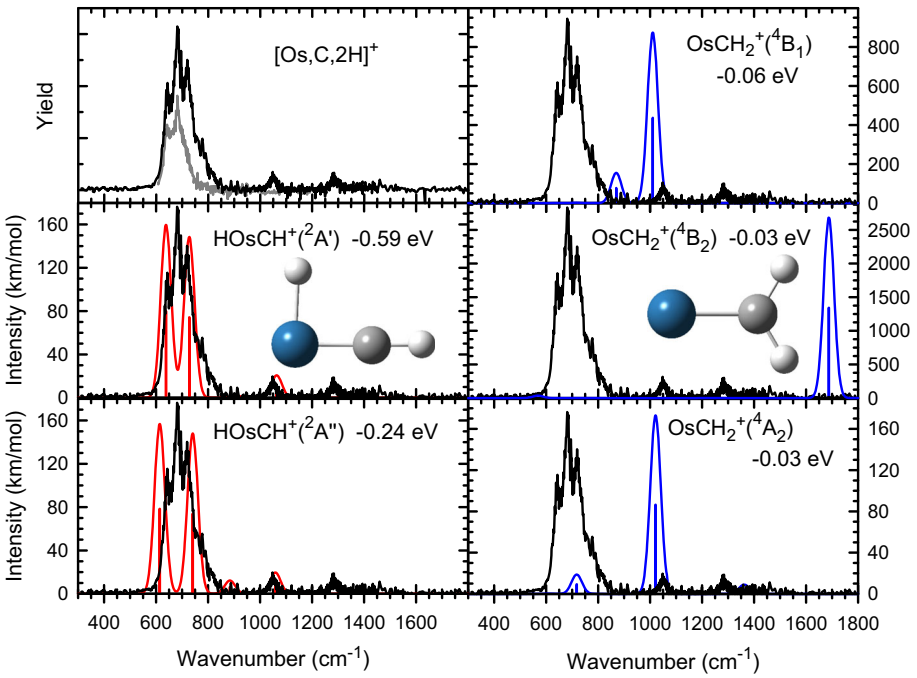

Figure 1. IRMPD spectrum for $[Os,C,2H]^+$ (black, in-focus; top left panel, out-of-focus, gray) and DFT calculated spectra for the doublet carbyne hydride (left middle and bottom traces, red) and quartet carbene (right traces, blue). The energies relative to $Os^+ + CH_4$ reactants from Table 1 and structures are also shown

nonbonding 5d orbitals: $1b_2^1 1a_2^1 2a_1^2$ for $^4B_1$, $1b_2^1 1a_2^2 2a_1^1$ for $^4B_2$, and $1b_2^2 1a_2^1 2a_1^1$ for $^4A_2$. (Each of these species also has a nonbonding 6s electron. The higher energy $^4B_1$ state listed in Table 1 has a nonbonding electron configuration of $1b_2^1 1a_2^1 2a_1^1 6s^2$.) None of the carbenes predict the broad intense band centered near 700 cm^{-1}. Further, none reproduce the weak band observed at 1286 cm^{-1}.

As noted above, we recently showed that consideration of the rotational band structure of the $[M,C,2D]^+$ species reproduced the experimentally observed spectra well for $M^+ = Ta^+$, W^+, Ir^+, and Pt^+ [45]. Figure 2 shows the predictions for the two $HOsCH^+$ species as well as the lowest energy carbene. It should be noted that to better match the observed spectra, the lowest energy band for the $HOsCH^+$ ($^2A'$) ground state has been blue-shifted by 30 cm^{-1}. (The spectrum without this shift is provided in the Supplementary Figure S4.) This shift is similar to that found in our examination of the comparable spectrum for $DIrCD^+$, where the lowest frequency band was shifted up by about 50 cm^{-1} in order to reproduce experiment with fidelity. Now that the rotational band structure is included, the broadband between 600 and 800 cm^{-1} can be attributed to overlap of the branches of the two bands centered at 638 and 728 cm^{-1} in the $^2A'$ ground state. We assign the peak observed at 649 cm^{-1} to the low-frequency branch of the b-type in-plane bend predicted at 638 cm^{-1}. The prominent central peak observed at 684 cm^{-1} is explained by overlap of the high-frequency branch of the in-plane bend and the low-frequency branch of the OsCH oop bend (c-type) predicted at 728 cm^{-1}. The 721 cm^{-1} maximum can then be assigned to the low K_a Q-branches of the oop bend, with the high-frequency branch explaining the shoulder at 770 cm^{-1}. The peak observed at 1049 cm^{-1} is attributed to the narrow P and R branches of the Os-C stretch (a-type) at 1064 cm^{-1}. Clearly, the broadband associated with the intense peak of the $OsCH_2^+$ ($^4B_2$) carbene (b-type) is inconsistent with the resonance observed at 1049 cm^{-1}. One could reason that application of a shift to the lowest band of the $^2A''$ species would also allow it to compare favorably to the observed spectrum; however, this shift would have to be substantially larger, about 60 cm^{-1}. Furthermore, the experimental peak at 721 cm^{-1} is reproduced better by the Q branch of the 728 cm^{-1} band of the $^2A'$ species than by the Q branch of the 741 cm^{-1} band of the $^2A''$ species. Naturally, minor contributions from the $^2A''$ state cannot be excluded, especially considering the exothermic nature of its predicted formation. The peak at 1286 cm^{-1} remains unexplained except possibly as an overtone of the 638 cm^{-1} band, in which case it would be a-type, consistent with the narrow resonance observed.

[Os,C,2D]+

Support for the assignments above comes from analysis of the IRMPD spectrum of $[Os,C,2D]^+$, shown in Figure 3. Again, a strong triplet of peaks is observed, but now at 461, 498, and 563 cm^{-1}, with two additional peaks of moderate intensity at 920 and 990 cm^{-1}, and a weak band at 1528 cm^{-1}. Figure 3 shows the comparison to the theoretical spectra for all species that can be formed exothermically from $Os^+ + CD_4$ reactants along with the lowest energy $^4B_1$ state of $OsCD_2^+$. As for the perprotio case, the $OsCD_2^+$ ($^4B_1$)

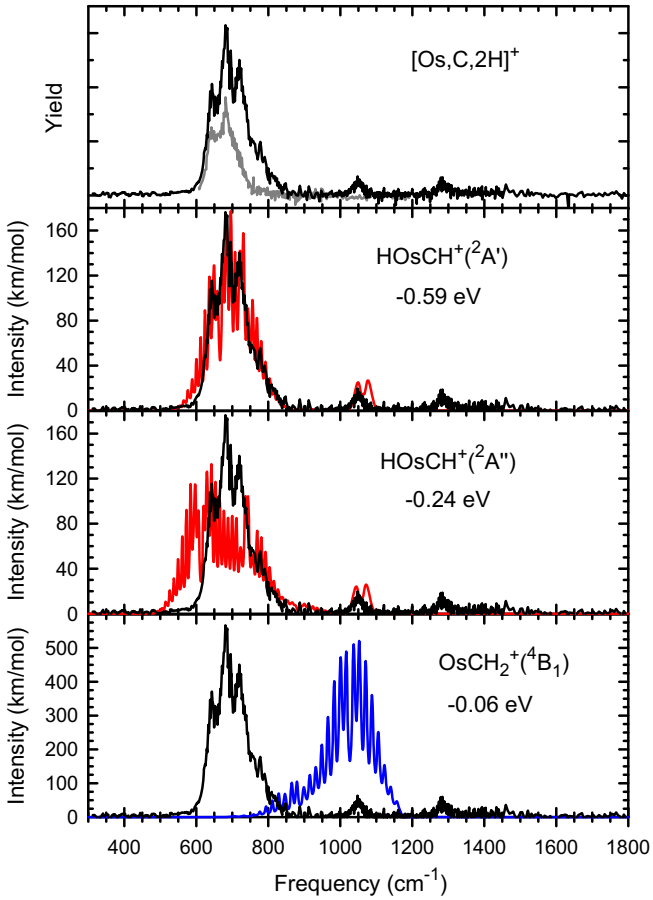

Figure 2. IRMPD spectra for $[Os,C,2H]^+$ (black, in-focus; top panel, out-of-focus, gray) and the DFT calculated spectra including rotational band structure for the doublet carbyne hydride (middle two traces, red) and quartet carbene (bottom trace, blue). The energies relative to $Os^+ + CH_4$ reactants from Table 1 are also included. The lowest frequency band of the $HOsCH^+$ ($^2A'$) species has been blue-shifted by 30 cm^{-1}

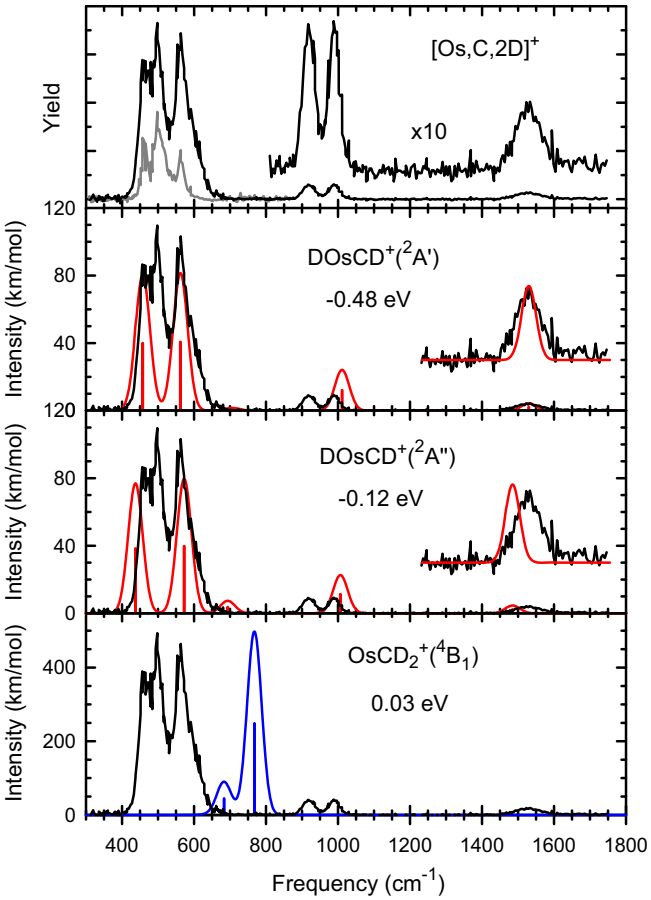

Figure 3. IRMPD spectra for $[Os,C,2D]^+$ (black, in-focus; top panel, out-of-focus, gray) and the DFT calculated spectra for the doublet carbyne deuteride (middle traces, red) and quartet carbene (bottom trace, blue). The energies relative to $Os^+ + CD_4$ reactants from Table 1 are also included

does not reproduce the most intense bands in the experimental spectrum (nor do the other two carbene states), whereas the carbyne deuteride structures do. As for the perprotio case, the separation between the bands at 457 and 561 cm^{-1} (the out-of-phase in-plane bend and OsCD out-of-plane bend, respectively) of the $^2A'$ state reproduces the width of the intense experimental band better than the larger separation between the analogous 437 and 571 cm^{-1} bands of the $^2A''$ state.

Comparison with the predicted spectrum including rotational contours of the $DOsCD^+$ ($^2A'$) ground state, shown in Figure 4, reproduces the intense broad band well. The two lowest frequency peaks correspond to the low- and high-frequency branches of the band calculated at 457 cm^{-1} (and again blue-shifted by 30 cm^{-1}; the spectrum without the 30 cm^{-1} shift is provided in the Supplementary Figure S5.) The peak at 563 cm^{-1} is attributed to the low K_a Q-branches of the band predicted at 561 cm^{-1}, and the breadth of this peak to the blue is accounted for by the high-frequency branch. As for the perprotiated species, the predicted spectrum for the $^2A'$ state provides a more accurate prediction of the observed spectrum compared to that for the low-lying $^2A''$ state, although a shift of about 50 cm^{-1} in the band predicted at 437 cm^{-1} would reproduce the experimentally observed triplet of peaks near 500 cm^{-1}. Further, for the perdeuterated species, the in-phase in-plane bend at 693 cm^{-1} is more intense than the comparable band for the $^2A'$ state (707 cm^{-1}) and should potentially be visible, whereas no intensity in this region is observed experimentally.

The two peaks at 920 and 990 cm^{-1} are assigned to the P and R-branches of the Os-C stretch (a-type), calculated to lie at 1011 cm^{-1}. Clearly, this assignment explains the matching intensities and widths of these two peaks, although the observed splitting (70 cm^{-1}) is larger than the predicted splitting (26 cm^{-1}). Similar observations were made in the analogous band of the $DIrCD^+$ ground state [45]. There, the discrepancy between the center of the two experimental peaks (the nonexistent Q-branch) and the predicted vibrational frequency was 40 cm^{-1} compared to the 56 cm^{-1}

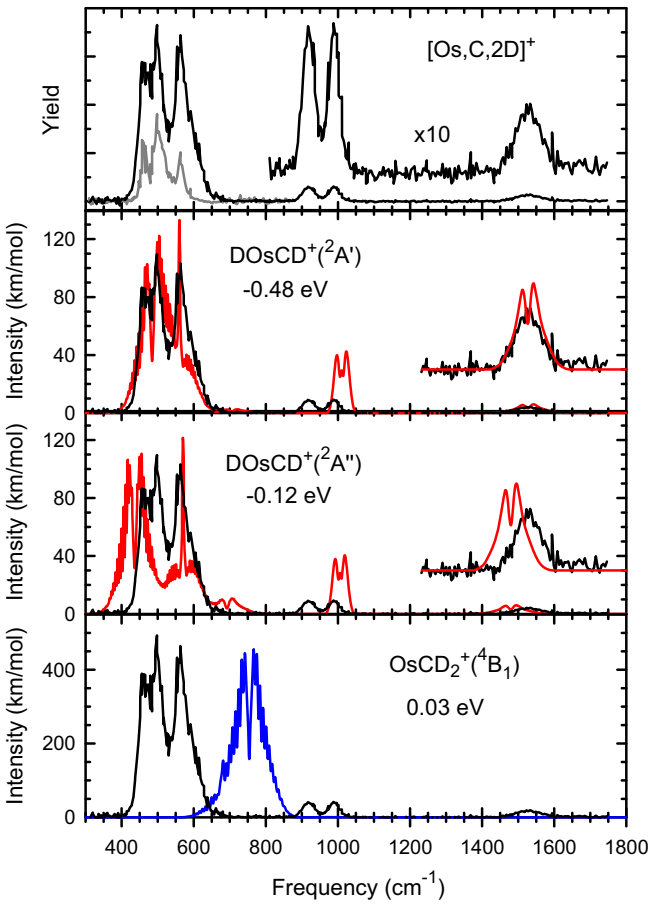

Figure 4. IRMPD spectra for $[Os,C,2D]^+$ (black, in-focus; top panel, out-of-focus, gray) and the DFT calculated spectra including rotational band structure for the doublet carbyne deuteride (middle traces, red) and quartet carbene (bottom trace, blue). The energies relative to $Os^+ + CD_4$ reactants from Table 1 are also included. The lowest frequency band of the $DOsCD^+(^2A')$ species has been blue-shifted by 30 cm^{-1}

observed here. (The shift is actually more similar because a scaling factor of 0.939 was used in the iridium system instead of 0.95 here.) In addition, for $DIrCD^+$, the observed splitting was 63 cm^{-1} compared to 70 cm^{-1} observed here (with the predicted splitting again being much smaller, 26 cm^{-1}). As noted in that work, the separation calculated between these two branches increases with temperature such that the large exothermicity for forming the $DOsCD^+$ and $DIrCD^+$ species could contribute to the larger separation observed. The weak band at 1528 cm^{-1} is reproduced well by the rotational band structure of the Os-D stretch (b-type) at 1528 cm^{-1} for the $^2A'$ ground state, less so by the 1481 cm^{-1} band predicted for the $^2A''$ excited state. (Although this could be attributed to the chosen scale factor, agreement would require scaling by 0.98 rather than 0.95, which would also shift all other bands, notably the 571 cm^{-1} band that presently reproduces the experimental peak at 563 cm^{-1}.) The CD stretch predicted at 2256 and 2246 cm^{-1} for the $^2A'$ and $^2A''$ species, respectively, is out of experimental range. In conclusion, we assign the observed spectrum to the $^2A'$ ground state, especially considering that the energetics are even more strongly biased to it than for the perprotio system. Finally, we note that if an overtone of the out-of-phase in-plane bend were to be observed, it would occur at about $2 \times (457 + 30) = 974$ cm^{-1} and thus could lie underneath the band observed at 990 cm^{-1}.

A reviewer wonders whether the band at 920 cm^{-1} might be assigned exclusively to the overtone and the 990 cm^{-1} band to unresolved P and R branches of the Os-C stretch. Although there is no way to be definitive about the assignment, we believe that this interpretation is probably not correct for several reasons. (a) It does not explain why the 920 and 990 cm^{-1} bands have identical intensities and widths, whereas the separated P and R branches of the Os-C stretch explain this easily. (b) It does not explain why this system exactly parallels observations made for the $DIrCD^+$ in the same spectral region: two bands of equal intensity and linewidth separated by similar amounts and shifted to slightly higher frequencies, consistent with the calculated M-C stretching frequencies (1021 cm^{-1} for Ir and 1011 cm^{-1} for Os when scaled by 0.950).

Conclusion

IRMPD action spectra of the products formed by dehydrogenation of methane and perdeuterated methane by osmium cations were measured over the 300–1800 cm^{-1} spectral range. The $[Os,C,2H]^+$ and $[Os,C,2D]^+$ experimental spectra agree well with those calculated for the ground state structures, the doublet carbyne hydride ($^2A'$). No evidence for the quartet spin carbene species is found. Comparison between experiment and theory is greatly enhanced by including the complete rotational band structure in the calculated spectra. As in a previous study [45], this result demonstrates that the rotational contours of small molecular systems can have appreciable effects on the appearance of IRMPD spectral bands explaining both the broadness of several bands and the doublet structures observed in others. In this regard, the observation of similar spectral signatures for $DOsCD^+$ and $DIrCD^+$ provides enhanced confidence in the assignments made for both species.

Acknowledgements

The Center for High Performance Computing (CHPC) at the University of Utah is acknowledged for their generous allocation of computing time.

Funding Information

We gratefully acknowledge the Nederlandse Organisatie voor Wetenschappelijk Onderzoek (NWO) for support of the FELIX Laboratory and support for this project was provided by the National Science Foundation, Grant Nos. CHE-1664618 and OISE-1357887.

References

1. Bharadwaj, S.S., Schmidt, L.D.: Catalytic partial oxidation of natural-gas to syngas. Fuel Process. Technol. **42**, 109–127 (1995)
2. Lee, Y.J., Hong, S.I., Moon, D.J.: Studies on the steam and CO_2 reforming of methane for GTL-FPSO applications. Catal. Today. **174**, 31–36 (2011)
3. Schwarz, H.: Chemistry with methane: concepts rather than recipes. Angew. Chem. Int. Ed. **50**, 10096–10115 (2011)
4. Roithová, J., Schröder, D.: Selective activation of alkanes by gas-phase metal ions. Chem. Rev. **110**, 1170–1211 (2010)
5. Allison, J.: The gas-phase chemistry of transition-metal ions with organic molecules. Prog. Inorg. Chem. **34**, 627–676 (1986)
6. Squires, R.R.: Gas-phase transition-metal negative ion chemistry. Chem. Rev. **87**, 623–646 (1987)
7. Aristov, N., Armentrout, P.B.: Methane activation by V^+: electronic and translational energy dependence. J. Phys. Chem. **91**, 6178–6188 (1987)
8. Sunderlin, L.S., Armentrout, P.B.: Methane activation by Ti^+: electronic and translational energy dependence. J. Phys. Chem. **92**, 1209–1219 (1988)
9. Schultz, R.H., Elkind, J.L., Armentrout, P.B.: Electronic effects in C-H and C-C bond activation: state-specific reactions of $Fe^+(^6D, ^4F)$ with methane, ethane, and propane. J. Am. Chem. Soc. **110**, 411–423 (1988)
10. Georgiadis, R., Armentrout, P.B.: Translational and electronic energy dependence of chromium ion reactions with methane. J. Phys. Chem. **92**, 7067–7074 (1988)
11. Sunderlin, L.S., Armentrout, P.B.: Periodic trends in chemical reactivity: reactions of Sc^+, Y^+, La^+, and Lu^+ with methane and ethane. J. Am. Chem. Soc. **111**, 3845–3855 (1989)
12. Russell, D.H.: Gas Phase Inorganic Chemistry. Plenum, New York (1989)
13. Eller, K., Schwarz, H.: Organometallic chemistry in the gas phase. Chem. Rev. **91**, 1121–1177 (1991)
14. Chen, Y.-M., Armentrout, P.B.: Activation of methane by gas-phase Rh^+. J. Phys. Chem. **99**, 10775–10779 (1995)
15. Armentrout, P.B., Kickel, B.L.: Gas-phase thermochemistry of transition metal ligand systems: reassessment of values and periodic trends. In: Freiser, B.S. (ed.) Organometallic Ion Chemistry, pp. 1–45. Kluwer, Dordrecht (1996)
16. Haynes, C.L., Chen, Y.-M., Armentrout, P.B.: The potential energy surface for activation of methane by Co^+: an experimental study. J. Phys. Chem. **99**, 9110–9117 (1995)
17. Haynes, C.L., Chen, Y.-M., Armentrout, P.B.: The reaction of $FeCH_2^+ + D_2$: probing the $[FeCH_4]^+$ potential energy surface. J. Phys. Chem. **100**, 111–119 (1996)
18. Chen, Y.-M., Sievers, M.R., Armentrout, P.B.: Activation of CH_4, C_2H_6, C_3H_8, and c-C_3H_6 by gas-phase Pd^+ and the thermochemistry of Pd-ligand complexes. Int. J. Mass Spectrom. Ion Process. **167/168**, 195–212 (1997)
19. Armentrout, P.B.: Gas phase organometallic chemistry. In: Brown, J.M., Hofmann, P. (eds.) Topics in Organometallic Chemistry, vol. 4, pp. 1–45. Springer-Verlag, Berlin (1999)
20. Sievers, M.R., Chen, Y.-M., Haynes, C.L., Armentrout, P.B.: Activation of CH_4, C_2H_6, and C_3H_8 by gas-phase Nb^+ and the thermochemistry of Nb-ligand complexes. Int. J. Mass Spectrom. **195/196**, 149–170 (2000)
21. Armentrout, P.B., Sievers, M.R.: Activation of CH_4 by gas-phase Zr^+ and the thermochemistry of Zr ligand complexes. J. Phys. Chem. A. **107**, 4396–4406 (2003)
22. Liu, F., Zhang, X.-G., Armentrout, P.B.: Activation of CH_4 by gas-phase Ni^+ and the thermochemistry of Ni ligand complexes. Phys. Chem. Chem. Phys. **7**, 1054–1064 (2005)
23. Armentrout, P.B.: Activation of CH_4 by gas-phase Mo^+ and the thermochemistry of Mo-ligand complexes. J. Phys. Chem. A. **110**, 8327–8338 (2006)
24. Shayesteh, A., Lavrov, V.V., Koyanagi, G.K., Bohme, D.K.: Reactions of atomic cations with methane: gas phase room-temperature kinetics and periodicities in reactivity. J. Phys. Chem. A. **113**, 5602–5611 (2009)
25. Irikura, K.K., Beauchamp, J.L.: Osmium tetroxide and its fragment ions in the gas phase: reactivity with hydrocarbons and small molecules. J. Am. Chem. Soc. **111**, 75–85 (1989)
26. Buckner, S.W., MacMahon, T.J., Byrd, G.D., Freiser, B.S.: Gas-phase reactions of Nb^+ and Ta^+ with alkanes and alkenes. C-H bond activation and ligand-coupling mechanisms. Inorg. Chem. **28**, 3511–3518 (1989)
27. Irikura, K.K., Beauchamp, J.L.: Electronic structure considerations for methane activation by third-row transition-metal ions. J. Phys. Chem. **95**, 8344–8351 (1991)
28. Irikura, K.K., Beauchamp, J.L.: Methane oligomerization in the gas phase by third-row transition-metal ions. J. Am. Chem. Soc. **113**, 2769–2770 (1991)
29. Zhang, X.-G., Liyanage, R., Armentrout, P.B.: The potential energy surface for activation of methane by Pt^+: a detailed guided-ion beam study. J. Am. Chem. Soc. **123**, 5563–5575 (2001)
30. Armentrout, P.B., Shin, S., Liyanage, R.: Guided-ion beam and theoretical study of the potential energy surface for activation of methane by W^+. J. Phys. Chem. A. **110**, 1242–1260 (2006)
31. Li, F.-X., Zhang, X.-G., Armentrout, P.B.: The most reactive third-row transition metal: guided ion beam and theoretical studies of the activation of methane by Ir^+. Int. J. Mass Spectrom. **255/256**, 279–300 (2006)
32. Parke, L.G., Hinton, C.S., Armentrout, P.B.: Experimental and theoretical studies of the activation of methane by Ta^+. J. Phys. Chem. C. **111**, 17773–17787 (2007)
33. Armentrout, P.B., Parke, L., Hinton, C., Citir, M.: Activation of methane by Os^+: guided ion beam and theoretical studies. ChemPlusChem. **78**, 1157–1173 (2013)
34. Armentrout, P.B.: Methane activation by 5d transition metals: energetics, mechanisms, and periodic trends. Chem. Eur. J. **23**, 10–18 (2017)
35. Armentrout, M.M., Li, F.-X., Armentrout, P.B.: Is spin conserved in heavy metal systems? Experimental and theoretical studies of the reaction of Re^+ with methane. J. Phys. Chem. A. **108**, 9660–9672 (2004)
36. Parke, L.G., Hinton, C.S., Armentrout, P.B.: Why is hafnium so unreactive? Experimental and theoretical studies of the reaction of Hf^+ with methane. Int. J. Mass Spectrom. **254**, 168–182 (2006)
37. Parke, L.G., Hinton, C.S., Armentrout, P.B.: Energetics and mechanisms of C-H bond activation by a doubly-charged metal ion: guided ion beam and theoretical studies of $Ta^{2+} + CH_4$. J. Phys. Chem. A. **112**, 10469–10480 (2008)
38. Li, F.-X., Armentrout, P.B.: Activation of methane by gold cations: guided ion beam and theoretical studies. J. Chem. Phys. **125**, 133114 (2006)
39. Irikura, K.K., Goddard III, W.A.: Energetics of third-row transition metal methylidene ions MCH_2^+ (M = La, Hf, Ta, W, Re, Os, Ir, Pt, Au). J. Am. Chem. Soc. **116**, 8733–8740 (1994)
40. Simon, A., Lemaire, J., Boissel, P., Maître, P.: Competition between Agostic WCH_2^+ and $HWCH^+$: a joint experimental and theoretical study. J. Chem. Phys. **115**, 2510–2518 (2001)
41. Schrock, R.R.: Alkylidene complexes of niobium and tantalum. Acc. Chem. Res. **12**, 98–104 (1979)
42. Goddard, R.J., Hoffmann, R., Jemmis, E.D.: Unusual metal-carbon-hydrogen angles, carbon-hydrogen bond activation, and -hydrogen abstraction in transition-metal carbene complexes. J. Am. Chem. Soc. **102**, 7667–7676 (1980)
43. Brookhart, M., Green, M.L.H.: Carbon-hydrogen–transition metal bonds. J. Organomet. Chem. **250**, 395–408 (1983)
44. Lapoutre, V.J.F., Redlich, B., van der Meer, A.F.G., Oomens, J., Bakker, J.M., Sweeney, A., Mookherjee, A., Armentrout, P.B.: Structures of the dehydrogenation products of methane activation by 5d transition metal cations. J. Phys. Chem. A. **117**, 4115–4126 (2013)
45. Owen, C.J., Boles, G.C., Chernyy, V., Bakker, J.M., Armentrout, P.B.: Structures of the dehydrogenation products of methane activation by 5d transition metal cations revisited: deuterium labeling and rotational contours. J. Chem. Phys. **148**, 044307 (2018)
46. Wheeler, O.W., Salem, M., Gao, A., Bakker, J.M., Armentrout, P.B.: Activation of C-H bonds in $Pt^+ + xCH_4$ reactions, where x = 1 – 4: identification of the platinum dimethyl cation. J. Phys. Chem. A. **120**, 6216–6227 (2016)
47. Letokhov, V.S., Ryabov, E.A., Tumanov, O.A.: Luminiscence of a molecular gas under the action of CO_2 laser pulses. Sov. Phys. JETP. **36**, 1069–1073 (1973)
48. Campbell, J.D., Hancock, G., Halpern, J.B., Welge, K.H.: Off resonant dissociation of NH_3 to ground state fragments by pulsed CO_2 laser radiation. Chem. Phys. Lett. **44**, 404–410 (1976)
49. Bakker, J.M., Lapoutre, V.J.F., Redlich, B., Oomens, J., Sartakov, B.G., Fielicke, A., von Helden, G., Meijer, G., van der Meer, A.F.G.: Intensity-resolved IR multiple photon ionization and fragmentation of C_{60}. J. Chem. Phys. **132**, 074305 (2010)

50. Lehmann, K.K., Scoles, G., Pate, B.H.: Intramolecular dynamics from eigenstate-resolved infrared-spectra. Annu. Rev. Phys. Chem. **45**, 241–274 (1994)
51. Beil, A., Luckhaus, D., Quack, M., Stohner, J.: Intramolecular vibrational redistribution and unimolecular reaction: concepts and new results on the femtosecond dynamics and statistics in CHBrClF. Ber. Bunsenges. Phys. Chem. **101**, 311–328 (1997)
52. Brümmer, M., Kaposta, C., Santambrogio, G., Asmis, K.R.: Formation and photodepletion of cluster ion-messenger atom complexes in a cold ion trap: infrared spectroscopy of VO^+, VO_2^+, and VO_3. J. Chem. Phys. **119**, 12700–12703 (2003)
53. Holthausen, M.C., Heinemann, C., Cornehl, H.H., Koch, W., Schwartz, H.: The performance of density-functional/Hartree-Fock hybrid methods: cationic transition-metal methyl complexes MCH_3^+. J. Chem. Phys. **102**, 4931 (1995)
54. Zhang, G., Li, S., Jiang, Y.: Dehydrogenation of methane by gas-phase Os^+: a density functional study. Organomet. **22**, 3820–3830 (2003)
55. Dietz, T.G., Duncan, M.A., Powers, D.E., Smalley, R.E.: Laser production of supersonic metal cluster beams. J. Chem. Phys. **74**, 6511–6512 (1981)
56. Haertelt, M., Lapoutre, V.J.F., Bakker, J.M., Redlich, B., Fielicke, A., Meijer, G.: Structure determination of anionic metal clusters via infrared resonance enhanced multiple photon electron detachment spectroscopy. J. Phys. Chem. Lett. **2**, 1720–1724 (2011)
57. Lemaire, J., Boissel, P., Heninger, M., Mauclaire, G., Bellec, G., Mestdagh, H., Le Caer, S., Ortega, J., Glotin, F., Maître, P.: Gas phase infrared spectroscopy of selectively prepared ions. Phys. Rev. Lett. **89**, 273002 (2002)
58. Bakker, J.M., Besson, T., Lemaire, J., Scuderi, D., Maître, P.: Gas-phase structure of a π-allyl-palladium complex: efficient infrared spectroscopy in a 7T Fourier transform mass spectrometer. J. Phys. Chem. A. **111**, 13415–13424 (2007)
59. Frisch, M.J., Trucks, G.W., Schlegel, H.B., Scuseria, G.E., Robb, M.A., Cheeseman, J.R., Scalmani, G., Barone, V., Petersson, G.A., Nakatsuji, H., Li, X., Caricato, M., Marenich, A.V., Bloino, J., Janesko, B.G., Gomperts, R., Mennucci, B., Hratchian, H.P., Ortiz, J.V., Izmaylov, A.F., Sonnenberg, J.L., Williams-Young, D., Ding, F., Lipparini, F., Egidi, F., Goings, J., Peng, B., Petrone, A., Henderson, T., Ranasinghe, D., Zakrzewski, V.G., Gao, J., Rega, N., Zheng, G., Liang, W., Hada, M., Ehara, M., Toyota, K., Fukuda, R., Hasegawa, J., Ishida, M., Nakajima, T., Honda, Y., Kitao, O., Nakai, H., Vreven, T., Throssell, K., Montgomery Jr., J.A., Peralta, J.E., Ogliaro, F., Bearpark, M.J., Heyd, J.J., Brothers, E.N., Kudin, K.N., Staroverov, V.N., Keith, T.A., Kobayashi, R., Normand, J., Raghavachari, K., Rendell, A.P., Burant, J.C., Iyengar, S.S., Tomasi, J., Cossi, M., Millam, J.M., Klene, M., Adamo, C., Cammi, R., Ochterski, J.W., Martin, R.L., Morokuma, K., Farkas, O., Foresman, J.B., Fox, D.J.: Gaussian 16, Revision A.03. Gaussian, Inc., Wallingford CT (2016)
60. Becke, A.D.: Density-functional thermochemistry. III. The role of exact exchange. J. Chem. Phys. **98**, 5648–5652 (1993)
61. Lee, C., Yang, W., Parr, R.G.: Development of the Colle-Salvetti correlation-energy formula into a functional of the electron density. Phys. Rev. B. **37**, 785–789 (1988)
62. Andrae, D., Haeussermann, U., Dolg, M., Stoll, H., Preuss, H.: Energy-adjusted ab initio pseudopotentials for the second and third row transition elements. Theor. Chim. Acta. **77**, 123–141 (1990)
63. Kesharwani, M.K., Brauer, B., Martin, J.M.L.: Frequency and zero-point vibrational energy scale factors for double-hybrid density functionals (and other selected methods): can anharmonic force fields be avoided? J. Phys. Chem. A. **119**, 1701–1714 (2015)
64. Barone, V.: Anharmonic vibrational properties by a fully automated second-order perturbative approach. J. Chem. Phys. **122**, 014108 (2005)
65. Leo Meerts, W., Schmitt, M.: Application of genetic algorithms in automated assignments of high-resolution spectra. Int. Rev. Phys. Chem. **25**, 353–406 (2006)